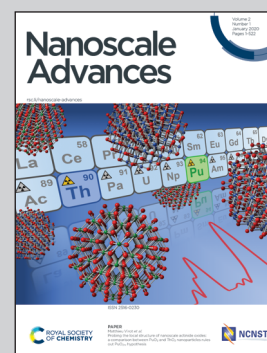**Showcasing research from the laboratory of Professor Jingyang Wang at Shenyang National Laboratory for Materials Science, Institute of Metal Research, Chinese Academy of Sciences, Shenyang, China.**

Boron nitride aerogels consisting of varied superstructures

Jingjing Pan and Jingyang Wang demonstrate a multilevel assembly scheme for the elegant fabrication of boron nitride aerogels consisting of varied superstructures, i.e. nanoribbons composed of tiny nanocrystals and nest-like structures tangled by nanofibers. Interestingly, the resultant aerogels exhibit great contrast in their hydrophilicity, which could be attributed to the microstructure difference.

ROYAL SOCIETY OF CHEMISTRY

rsc.li/nanoscale-advances

COMMUNICATION

Check for updates

Boron nitride aerogels consisting of varied superstructures†

Jingjing Pan [ab] and Jingyang Wang [*a]

As a porous material with a nanoscale skeleton, aerogel serves as a bridge between the nano- and macro-world. The integration of nanostructures into aerogels not only allows the combination of multidimensional features but also implies the possibility of unexpected properties. With great potential in many fields, boron nitride (BN) nanostructures have garnered growing attention and their existence in the aerogel state holds even more promise. However, the existing fabrication routes in the aerogel field, despite their validity and effectiveness, provide no panacea and are challenged by those incompatible with the current preparation toolbox, among which BN stands out. Herein, a multilevel assembly scheme is demonstrated for the elegant fabrication of BN aerogels consisting of varied superstructures, *i.e.*, nanoribbons composed of tiny nanocrystals and nest-like structures tangled by nanofibers, the realization of which *via* the traditional molecular route or the classic assembly route is rather difficult. Interestingly, the resultant aerogels were found to exhibit great contrast in their hydrophilicity, which could be attributed to the microstructure difference. This study may raise the prospects of BN in energy, environment, bio-applications, *etc.* It may also give inspirations for the incorporation of other complex structures into aerogels.

Aerogels have received tremendous attention owing to their unique porous structure, ultrahigh porosity, and low density, which enable multifarious applications such as environmental remediation, catalysis, and thermal insulation.[1–3] As the mainstay of the applications, fabrication is of great significance in this field. The existing methods for aerogel fabrication are mainly of two types.[4] The traditional one is the molecular route that utilizes molecular precursors, such as alkoxides or salts, some of which are either hazardous or highly costly. For many constituents, corresponding precursors do not even exist for gel

formation, which limit aerogels to very few varieties. This route yields aerogels consisting of covalent-bonded nanoparticles, which feature a typical string-of-pearl-like micromorphology, and it offers little scope for microstructure tailoring. Moreover, the resultant aerogels are usually in the amorphous state and the crystallization requires further high temperature treatment, which may destroy the integrated structure. In the late 1990s, researchers who pioneered the fabrication of chalcogenide aerogel contributed to the other brand-new fabrication strategy.[5–7] They gave up molecular precursors and employed ready-made nanocrystals as building blocks that were then assembled into 3D aerogels. In this assembly route, the formation of aerogel is driven by supramolecular forces and the integrated aerogel is maintained by non-covalent interactions. The microstructure is accordingly changeable due to the following two factors: (1) the diverse choices of building blocks (0D, 1D, and 2D low dimensional nanostructures); (2) the versatility of supramolecular interactions (hydrogen bonds, π–π stacking, and electrostatic interactions). In light of this method, the diversity of the aerogels is significantly extended and a growing number of aerogels have been successfully fabricated.[8] An epitome of the evolution of the fabrication routes is the carbon-based aerogel, which was once derived from carbonized organic aerogels[9] (molecular route) and has afterwards encompassed almost all the carbon nano-systems, such as carbon dots (0D), carbon nanotubes (1D), and graphene (2D) *via* the assembly route.[10–12]

Despite the spectacular success, the current assembly route is still not a panacea for aerogel fabrication. One problem, for example, is that many building blocks can hardly be assembled due to the lack of controllable surface functional groups. Even though possible with the assistance of foreign binders, the involvement of other substances may diminish the unique properties in the nanoscale and the binder is also inappropriate for those that hold promise in high-temperature applications. Furthermore, the fabrication of building blocks and the subsequent assembly process are separate parts in the current assembly route. Low dimensional nanostructures are often used

ᵃShenyang National Laboratory for Materials Science, Institute of Metal Research, Chinese Academy of Sciences, Shenyang, 110016, China. E-mail: jywang@imr.ac.cn

ᵇSchool of Materials Science and Engineering, University of Science and Technology of China, Hefei, 230026, China

as received, which means that the quality of the resultant aerogels relies heavily on the ready-made building blocks; therefore, the alteration of the overall properties mainly counts on the post procedures and could hardly be realized by the roots.

Isomorphic to carbon, BN and its corresponding nanostructures have garnered growing attention,[13–16] but it is also a primary example of those failing to fit in well with the current fabrication toolbox in the aerogel field. The first-reported BN aerogel was prepared *via* the molecular route,[17] following the step for preparing carbon aerogel, whereas its practical applications were hindered by hazardous chemicals and arduous procedures. Recently, BN aerogels assembled from exfoliated BN nanosheets were reported and the overall samples were maintained by van der Waals force or organic binders.[18–20] On the other hand, BN aerogels directly assembled from BN dots or BN nanotubes are yet to be achieved, which may be due to difficulty in the assembly process and scalable production of varied BN building blocks. Besides the above routes, employing other aerogels as templates was also explored, which adds to the diversity of BN aerogel microstructures and unlocks their high temperature applications.[21–25] However, template deposition may only serve as a short-term expedient. More recently, efficient fabrication of BN aerogels with nanoribbon-tangled networks was also achieved.[26,27] Nonetheless, the diversity of BN aerogels still lags behind that of their carbon counterparts and there lacks a complementary strategy compatible with the current fabrication methodology in the aerogel field.

In view of the current situation, we demonstrate herein another fabrication scheme, the general idea of which is illustrated in Fig. 1. Compared with the current assembly route, this scheme features an extra assembly at the molecular level, which offers great scope for microstructure tailoring. It also involves molecular precursors but they could assemble into different motifs at first and the resultant aerogels derived from them are not limited to the string-of-pearl-like microstructure, which distinguishes this scheme from the traditional molecular route. Since the fabrication of the target building blocks and the processing of aerogel are not apart but synchronous, the control over the performance of the resultant aerogels could be exerted by the roots. Further explanations for this scheme can be found in the ESI.†

As a proof of concept, we realized the elegant fabrication of boron nitride (BN) aerogels consisting of varied superstructures: nanoribbons composed of tiny nanocrystals and nest-like structures tangled by nanofibers. In this work, we used several molecular building blocks, *i.e.*, melamine (M), acetoguanamine (M*), and boric acid (B) as raw molecules. Among them, melamine and boric acid have long been recognized as cheap precursors for BN. Additionally, M*, which is like M, was also selected in this work, and the only difference between these two molecules is that M has all three amino groups connected with the triazine ring, whereas M* has one amino group replaced by a methyl group. Given that melamine and its derivatives are versatile in supramolecular assembly, which enables the formation of different motifs *via* hydrogen bonds,[28] we attempted to use different molecular building blocks to form varied low dimensional structures at first. Then, they were tangled to form supramolecular gels, which were subsequently converted to the final aerogels. In a typical synthesis, the raw molecular building blocks were dissolved in hot water and the supramolecular gels formed as the systems cooled down. Since the gel formation was driven by non-covalent interactions, these
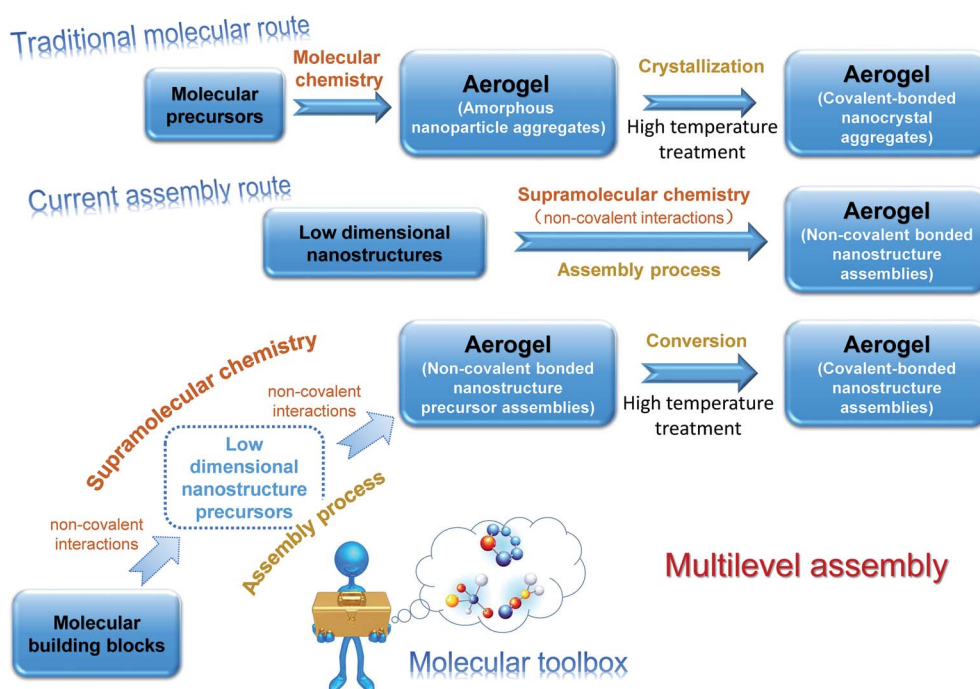

Fig. 1 Illustration of the multilevel assembly scheme.

gels could recover the solution states (Fig. S1†). The wet gels were then freeze-dried and characterized by X-ray diffraction (XRD) and Fourier transform infrared spectroscopy (FTIR) (Fig. S2†). After a conversion process under high temperature, the final BN aerogels were obtained.

In one case (Fig. 2), melamine (M) and boric acid (B) were used as the molecular building blocks; their molar ratio was set at M : B = 1 : 2, M : B = 1 : 4, and M : B = 1 : 6. As depicted in Fig. 2a, the X-ray diffraction (XRD) patterns of the resultant aerogels suggest that all the samples show characteristic peaks of hexagonal BN (h-BN) at about 26.7°, 41.6°, 55.1°, and 75.9°, which can be ascribed to (0002), (10$\bar{1}$0), (0004), and (11$\bar{2}$0) planes, respectively. Moreover, it is noticeable that the crystallization of the aerogel increases and becomes optimum as the molar ratio of M to B changes from 1 : 2 to 1 : 6. For comparison, a typical pattern of the commercial h-BN powder is also included here. The scanning electronic microscopic (SEM) observations reveal that the supramolecular gels show a typical nanoribbon-tangled morphology despite the difference in the starting molar ratio (Fig. S3†). For brevity, we only present here the results of the sample obtained under the optimum condition, i.e., the sample with the starting molar ratio being set at M : B = 1 : 6. As shown in Fig. 2c, the as-obtained BN aerogel consists of tangled nanoribbons. Furthermore, the sample was also characterized by using transmission electron microscopy (TEM). It is interesting to note that the nanoribbons consist of finer overlapped nanocrystals that display various orientations, as revealed by the TEM analysis (Fig. 2d, e, and S4†). The clear lattice fringes observed in the high-resolution TEM image (Fig. 2e) display a layer spacing of 3.34 Å, which is in line with the planar distance of the (0002) planes for h-BN.

In addition, we also explored the possibility of using M* and B as molecular building blocks for the fabrication of BN aerogels. The starting molar ratio was still set at M* : B = 1 : 2, M* : B = 1 : 4, and M* : B = 1 : 6. However, the final products were not the expected integrated BN aerogels but merely scattered fragments, even though their XRD patterns (Fig. S5†) display similar trend as those for the samples derived from M and B (Fig. 2a). The SEM observations (Fig. S6†) reveal that the micromorphologies of the supramolecular gels assembled from M* and B are varied as the molar ratio changes: at M* : B = 1 : 2, a spherical flower-like structure aggregated by tiny ribbons was formed; with the molar ratio adjusted from M* : B = 1 : 2 to M* : B = 1 : 4 and finally to M* : B = 1 : 6, the original flower-like structure gradually got flattened. The SEM images with higher magnification (Fig. S6†) show that the tangled ribbons (around 200 nm in width) are narrower than those assembled from M and B (around 1 μm in width), as previously displayed in Fig. S3.†
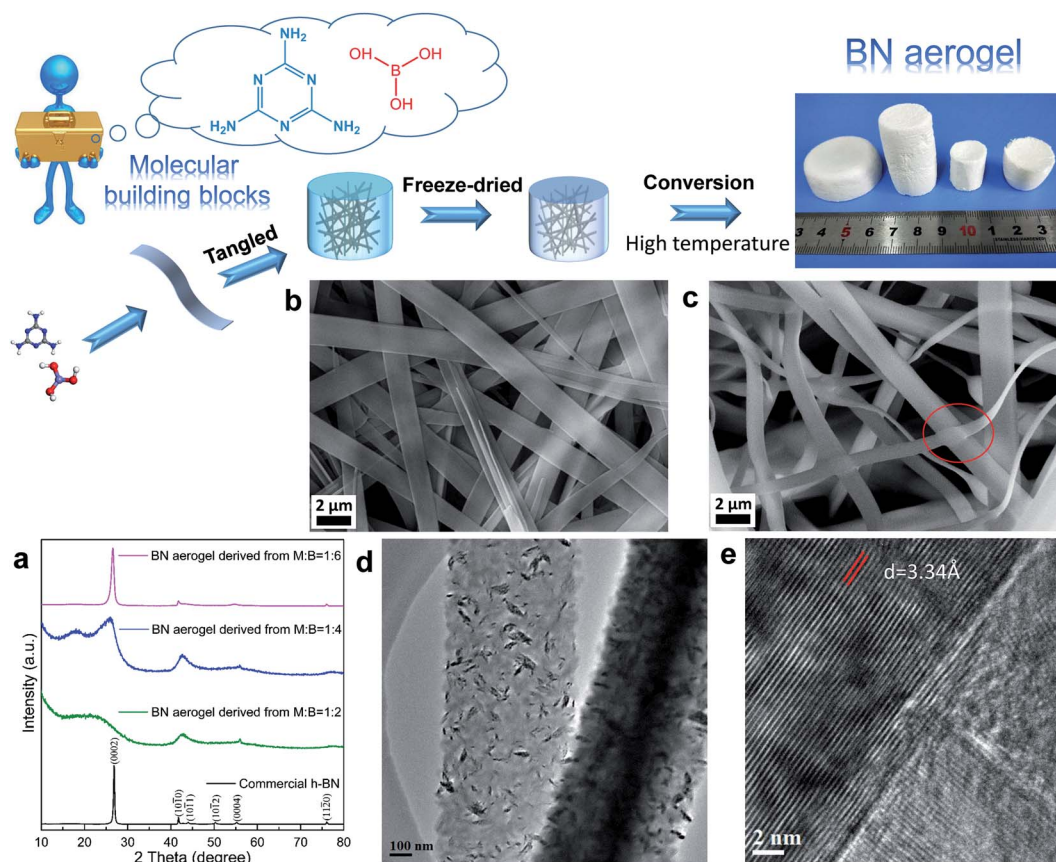

Fig. 2   Preparation of BN aerogel using melamine (M) and boric acid (B) as molecular building blocks. (a) XRD patterns of the resultant aerogels derived from M and B at different molar ratio; SEM images of the supramolecular precursor gel obtained at M : B = 1 : 6 (b) and the resultant BN aerogel (c); TEM results of the BN aerogel derived from M : B = 1 : 6 are displayed in (d) and (e).

These phenomena are understandable if we give consideration to the molecular structure of M*. As depicted in Fig. 3, M is a planar molecule that is surrounded by fascinating H-bonding sites, which could connect with boric acid molecules from all the directions *via* hydrogen-bonding interactions. But M* is different from M – as it has one amino group replaced by a methyl group, which offers no H-bonding sites. Herein, the involvement of the methyl group changes the number of H-bonding sites and influences the assembly pathways. For M, it could assemble with B and form a ribbon-like structure, as shown in the literature.[29,30] Compared with M, M* has less H-bonding sites and lower symmetry. When M* interacts with B, less bonding sites make the overall connection weaker, resulting in freeze-dried supramolecular gels that are very loose and the final products (after the conversion process under high temperature) are scattered fragments instead of integrated aerogels. For M*, different direction means different to the assembly process. As the methyl group provides no H-bonding sites, M* has less possibility to extend when it assembles with B; therefore, the as-formed nanoribbons are narrower than those made from M and B, as evidenced by the SEM results. Moreover, the assembly patterns are sensitive to the starting molar ratio. At lower amounts of B, *i.e.*, M* : B = 1 : 2, the as-formed nanoribbons aggregate into a spherical flower-like structure, which may favor the stability of the assembly system. As the amount of B increases, the assembly of M* and B is facilitated by more sufficient building blocks and the as-formed tangled nanoribbons tend to be flattened. Although M* and B were found to be

unsuitable for the fabrication of integrate BN aerogels, the above-mentioned findings lay the foundations for the following future explorations.

In the other case (Fig. 4), we started from melamine (M), acetoguanamine (M*), and boric acid (B). By involving both M and M*, we aimed to exploit the morphology transformation of M* and B without yielding the scattered fragments, given that M has ample H-bonding sites and it is favorable for the fabrication of integrated aerogels. The molar ratio of M : M* : B was kept at 1 : 1 : 2, 1 : 1 : 6, and 1 : 1 : 10. At M : M* : B = 1 : 1 : 2, a small amount of supramolecular gel was formed (Fig. S7a†), which could be ascribed to the insufficient building molecules, *i.e.*, the amount of B was too low. By putting the tiny gel fragments under SEM observation, it was found that the micromorphology was like ill-formed flowers (Fig. S7b†). Besides this, these gel fragments were also freeze-dried and underwent the subsequent conversion process under high temperature. The resultant powder was characterized *via* XRD and the diffraction peaks indicated the poor crystalline nature of the product (Fig. S7c†). The above factors made us abandon this experiment. In the next attempt, the starting molar ratio was set at M : M* : B = 1 : 1 : 6. Under this condition, the as-formed supramolecular gel exhibits a well-formed flower-like micromorphology, as displayed in Fig. 4a. Interestingly, we also observed a honeycomb structure in the SEM images (Fig. S8†). The resultant aerogel in this circumstance remains intact, proving that involving extra M could favor the formation of integrated aerogels without influencing the exploitation of
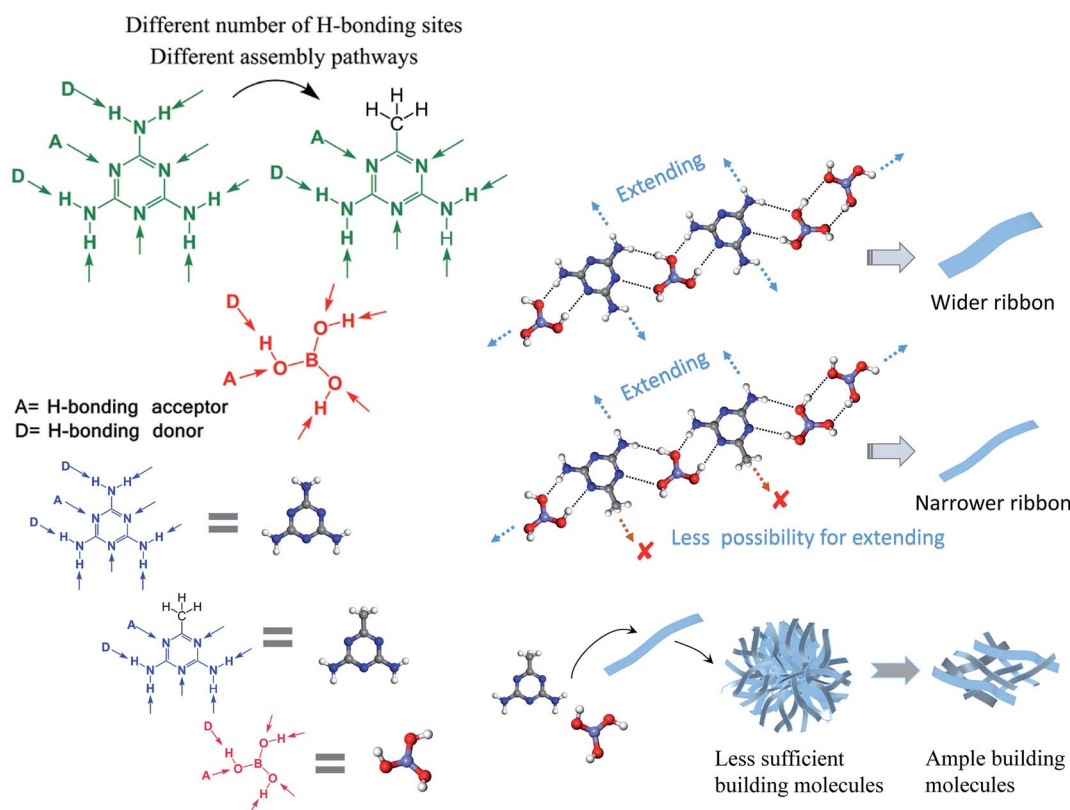

Fig. 3 Illustration of the H-bonding sites of melamine (M), acetoguanamine (M*), and boric acid (B), as well as their possible assembly pathways.
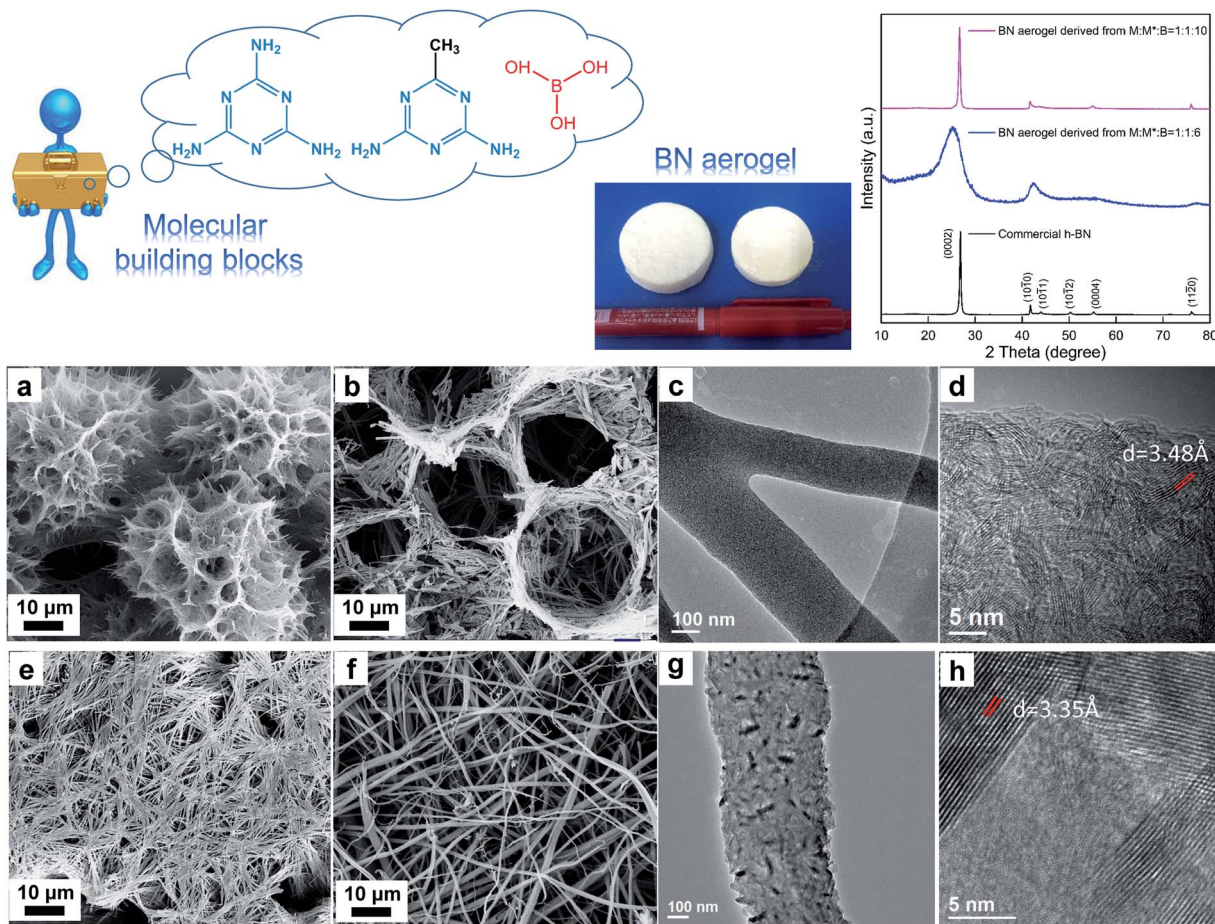
Fig. 4 Preparation of the BN aerogel with melamine (M), acetoguanamine (M*), and boric acid (B) as molecular building blocks. SEM images of the supramolecular precursor gel obtained at M : M* : B = 1 : 1 : 6 (a) and the corresponding BN aerogel (b); TEM results of the BN aerogel derived from M : M* : B = 1 : 1 : 6 are displayed in (c) and (d); SEM images of the supramolecular precursor gel obtained at M : M* : B = 1 : 1 : 10 (e) and the corresponding BN aerogel (f); TEM results of the BN aerogel derived from M : M* : B = 1 : 1 : 10 are displayed in (g) and (h).

unique morphology of M* and B supramolecular gels. The final BN aerogel shows a nest-like microstructure made of tiny ribbons (Fig. 4b); the TEM studies reveal that the ribbons are furcate (Fig. 4c) and the plane stripes are relatively random (Fig. 4d), with the layer spacing of about 3.48 Å, which is a bit larger than that of h-BN. Compared with h-BN, the XRD pattern of the sample derived from M : M* : B = 1 : 1 : 6 is less sharp and the diffraction peak of (0002) shifts a bit to a lower angle, indicative of larger interlayer distance, which is consistent with the TEM results. Based on the above studies, we can conclude that the phase composition of the resultant aerogel is primarily turbostractic BN (t-BN),[31] which has lower crystallization and less ordered stacking along the c-axis that is perpendicular to the (0002) planes, in comparison with h-BN. In our third attempt in this case, the starting molar ratio was set at M : M* : B = 1 : 1 : 10. In this circumstance, the as-obtained supramolecular gel displays a flattened network intertwined by tiny fibers (Fig. 4e), and the final BN aerogel could also remain intact and inherit this flattened structure (Fig. 4f). The TEM results show that the tiny fibers are made up of finer well-crystallized areas with different orientations (Fig. 4g, h, and

S9†). Also, the diffraction peaks in the corresponding XRD pattern are sharp and intense. The lattice fringes of the (0002) planes in the TEM images are clear and orderly arranged, with the interplanar distance measured to be 3.35 Å, which is in agreement with the value for h-BN.

Other information about the as-prepared BN aerogels in both cases such as density, porosity, and N_2 sorption results can be found in ESI (Table S2, Fig. S10†).

The above results show that the as-obtained BN aerogels exhibit different superstructures. It is generally believed that nanomaterials with a diverse structural hierarchy will outperform the individual subunits and even show unexpected properties.[32] Accordingly, these BN aerogels with unique microstructures may hold promise in many fields, such as energy storage, catalysis, or electronics, and even opens up new possibilities of applications.

It is worth mentioning that the as-prepared aerogels in this work exhibit a startling contrast in their water repellency (Fig. 5). The BN aerogel derived from M : B = 1 : 6 absorbed water instantly as it got close to the water drop (Video S1†) and its contact angle (CA) for water was measured to be 0°,
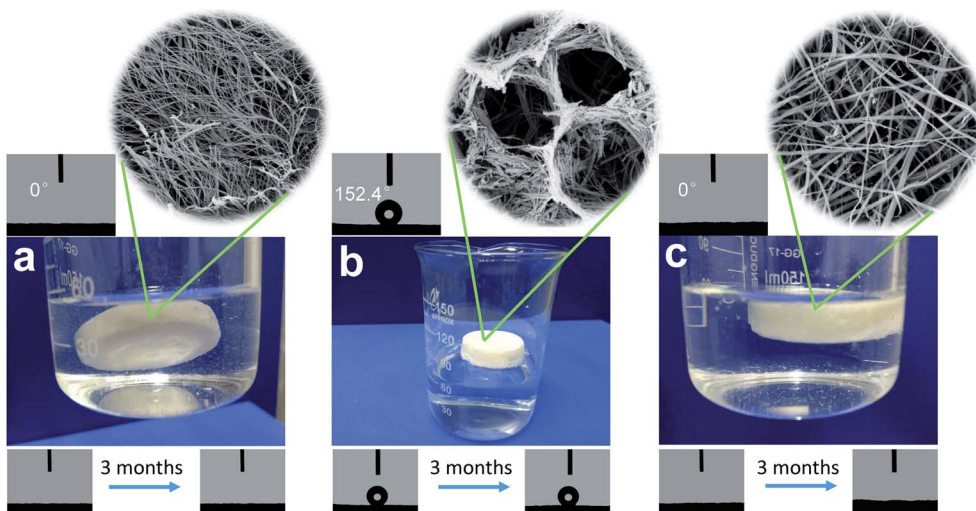
Fig. 5 The hydrophilicity of the BN aerogel derived from M : B = 1 : 6 (a), M : M* : B = 1 : 1 : 6 (b), and M : M* : B = 1 : 1 : 10 (c).

indicating that the sample is superhydrophilic (Fig. 5a). Other samples with M and B as raw molecules were found to exhibit the same phenomena, regardless of the difference in the starting molar ratio. When M, M*, and B were used as raw molecules, the BN aerogel derived from M : M* : B = 1 : 1 : 6 showed great repellency for water (Video S2†) and the CA was measured to be 152.4°, suggesting the superhydrophobic characteristic of the sample (Fig. 5b); the BN aerogel derived from M : M* : B = 1 : 1 : 10 exhibited great hydrophilicity, as displayed in Video S3† and Fig. 5c. Notably, the special wetting states of the BN aerogels were found to sustain for more than 3 months, thus exemplifying the robustness.

As is known to all, the wetting behavior of a surface is mainly governed by two factors, *i.e.*, chemical composition and surface geometry.[33] Based on the fact that the super-hydrophilic BN aerogels in this work share similar micromorphologies, whereas the superhydrophobic sample exhibits a considerably different microstructure (Fig. S11†), we postulated that the great contrast in the water repellency might originate from the microstructure difference. To gain more insight, X-ray photoelectron spectroscopic (XPS) analysis was conducted (Fig. S12†). Commercial h-BN was also included for comparison. The full survey scan XPS measurement suggests that B, N, C, and O elements were detected in all the samples. Also, the narrow scan spectra display more details about B and N elements. The B 1s spectra can be fitted into two peaks at 190.3 eV and 192.1 eV, which correspond to B–N and B–OH. The B–N signals arise from the main composition in the BN aerogel and the B–OH peaks may come from the decomposed boric acid. The N 1s spectra have a main peak at 397.9 eV, corresponding to N–B, which is in accordance with the main peak in the B 1s spectra, and the shoulder peak at 399.8 eV could be ascribed to N–H arising from the decomposition of melamine. The XPS results reveal that all the samples exhibit similar surface chemistry and the surface groups are hydrophilic, whereas not all of the aerogels show great affinity for water, implying that surface geometry outperforms chemical composition in influencing the apparent wettability of BN

aerogels in this work. To further confirm this, we pressed three samples into flat plates, during which the influence of the surface microstructure could be largely reduced. The CA tests show that all the plates display the same hydrophilicity (Fig. S13†). The above results led us to attribute the great contrast in hydrophilicity to microstructure difference.

BN nanomaterials have shown huge potential in many fields, such as environmental remediation,[34] water desalination,[35,36] or bio-applications,[37] just to name a few. Despite active endeavors, it is still challenging to realize different wettability on BN-related materials.[22,38–42] Also, there is a possibility that the as-obtained wetting states could only sustain for a short time.[22] Compared with the previous efforts, our work demonstrated not only the effective fabrication of the BN aerogel with varied microstructures but the tuning of wetting behavior without involving any special treatment, which are widely employed in wettability modulation, such as irradiation, etching, or coating.[33] This work may raise the prospects of BN for a wide range of applications.

In summary, we demonstrated a multilevel assembly scheme for the elegant fabrication of BN aerogels consisting of varied superstructures. A slight change in the molecular building blocks could make the final aerogels exhibit varied microstructures and distinctly different hydrophilicity: superhydrophilicity and superhydrophobicity. Besides the results described, there is still plenty of room for further explorations: the cause of complex structures, the detailed investigation of the superwetting states, and the possible applications of these BN aerogels with unique superstructures. Given that the molecular toolbox is far larger than we have exploited and the non-covalent interactions consist of more than H-bonds, it would be interesting to explore more possibilities about this scheme and attempts are currently ongoing in our laboratory. It is anticipated that the super-structured BN aerogels can find applications in many fields such as energy storage, environment remediation, or electronics, and the principle of this work may also inspire the fabrication of other aerogels with complex microstructures.

Conflicts of interest

There are no conflicts to declare.

Acknowledgements

Notes and references

1 H. Maleki, *Chem. Eng. J.*, 2016, **300**, 98–118.

2 H. Maleki and N. Huesing, *Appl. Catal., B*, 2018, **221**, 530–555.

3 R. Baetens, B. P. Jelle and A. Gustavsen, *Energy Build.*, 2011, **43**, 761–769.

4 F. Rechberger and M. Niederberger, *Nanoscale Horiz.*, 2017, **2**, 6–30.

5 T. Gacoin, L. Malier and J.-P. Boilot, *Chem. Mater.*, 1997, **9**, 1502–1504.

6 T. Gacoin, L. Malier and J.-P. Boilot, *J. Mater. Chem.*, 1997, **7**, 859–860.

7 L. Malier, J. P. Boilot and T. Gacoin, *J. Sol-Gel Sci. Technol.*, 1998, **13**, 61–64.

8 C. Ziegler, A. Wolf, W. Liu, A.-K. Herrmann, N. Gaponik and A. Eychmueller, *Angew. Chem., Int. Ed.*, 2017, **56**, 13200–13221.

9 R. W. Pekala, Low density, Resorcinol-Formaldehyde Aerogels, *US Pat.*, 4873218, 10 October 1989.

10 J. Wang and M. W. Ellsworth, in *Graphene and Emerging Materials for Post-Cmos Applications*, ed. Y. Obeng, S. DeGendt, P. Srinivasan, D. Misra, H. Iwai, Z. Karim, D. W. Hess and H. Grebel, 2009, vol. 19, pp. 241–247.

11 M. B. Bryning, D. E. Milkie, M. F. Islam, L. A. Hough, J. M. Kikkawa and A. G. Yodh, *Adv. Mater.*, 2007, **19**, 661.

12 L. X. Lv, Y. Q. Fan, Q. Chen, Y. Zhao, Y. Hu, Z. P. Zhang, N. Chen and L. T. Qu, *Nanotechnology*, 2014, **25**, 235401.

13 D. Golberg, Y. Bando, Y. Huang, T. Terao, M. Mitome, C. Tang and C. Zhi, *ACS Nano*, 2010, **4**, 2979–2993.

14 R. Arenal and A. Lopez-Bezanilla, *Wiley Interdiscip. Rev.: Comput. Mol. Sci.*, 2015, **5**, 299–309.

15 J. Yin, J. Li, Y. Hang, J. Yu, G. Tai, X. Li, Z. Zhang and W. Guo, *Small*, 2016, **12**, 2942–2968.

16 W. Luo, Y. Wang, E. Hitz, Y. Lin, B. Yang and L. Hu, *Adv. Funct. Mater.*, 2017, **27**, 1701450.

17 D. A. Lindquist, T. T. Borek, S. J. Kramer, C. K. Narula, G. Johnston, R. Schaeffer, D. M. Smith and R. T. Paine, *J. Am. Ceram. Soc.*, 1990, **73**, 757–760.

18 W. Lei, V. N. Mochalin, D. Liu, S. Qin, Y. Gogotsi and Y. Chen, *Nat. Commun.*, 2015, **6**, 8849.

19 X. Zeng, L. Ye, S. Yu, R. Sun, J. Xu and C.-P. Wong, *Chem. Mater.*, 2015, **27**, 5849–5855.

20 S. M. Jung, H. Y. Jung, M. S. Dresselhaus, Y. J. Jung and J. Kong, *Sci. Rep.*, 2012, **2**, 849.

21 M. Rousseas, A. P. Goldstein, W. Mickelson, M. A. Worsley, L. Woo and A. Zettl, *ACS Nano*, 2013, **7**, 8540–8546.

22 P. Thang, A. P. Goldstein, J. P. Lewicki, S. O. Kucheyev, C. Wang, T. P. Russell, M. A. Worsley, L. Woo, W. Mickelson and A. Zettl, *Nanoscale*, 2015, **7**, 10449–10458.

23 Y. Song, B. Li, S. Yang, G. Ding, C. Zhang and X. Xie, *Sci. Rep.*, 2015, **5**, 10337.

24 Y. Xue, P. Dai, M. Zhou, X. Wang, A. Pakdel, C. Zhang, Q. Weng, T. Takei, X. Fu, Z. I. Popov, P. B. Sorokin, C. Tang, K. Shimamura, Y. Bando and D. Golberg, *ACS Nano*, 2017, **11**, 558–568.

25 X. Xu, Q. Zhang, M. Hao, Y. Hu, Z. Lin, L. Peng, T. Wang, X. Ren, C. Wang, Z. Zhao, C. Wan, H. Fei, L. Wang, J. Zhu, H. Sun, W. Chen, T. Du, B. Deng, G. J. Cheng, I. Shakir, C. Dames, T. S. Fisher, X. Zhang, H. Li, Y. Huang and X. Duan, *Science*, 2019, **363**, 723.

26 J. Lin, X. Yuan, G. Li, Y. Huang, W. Wang, X. He, C. Yu, Y. Fang, Z. Liu and C. Tang, *ACS Appl. Mater. Interfaces*, 2017, **9**, 44732–44739.

27 G. Li, M. Zhu, W. Gong, R. Du, A. Eychmüller, T. Li, W. Lv and X. Zhang, *Adv. Funct. Mater.*, 2019, **29**, 1900188.

28 B. Roy, P. Bairi and A. K. Nandi, *RSC Adv.*, 2014, **4**, 1708–1734.

29 A. Roy, A. Choudhury and C. N. R. Rao, *J. Mol. Struct.*, 2002, **613**, 61–66.

30 Y. Atalay, D. Avci, A. Basoglu and I. Okur, *J. Mol. Struct.: THEOCHEM*, 2005, **713**, 21–26.

31 J. Thomas, N. E. Weston and T. E. O'Connor, *J. Am. Chem. Soc.*, 1962, **84**, 4619–4622.

32 L. Cong, H. Xie and J. Li, *Adv. Energy Mater.*, 2017, **7**, 1601906.

33 X. Feng and L. Jiang, *Adv. Mater.*, 2006, **18**, 3063–3078.

34 S. Yu, X. Wang, H. Pang, R. Zhang, W. Song, D. Fu, T. Hayat and X. Wang, *Chem. Eng. J.*, 2018, **333**, 343–360.

35 L. Garnier, A. Szymczyk, P. Malfreyt and A. Ghoufi, *J. Phys. Chem. Lett.*, 2016, **7**, 3371–3376.

36 S. Dervin, D. D. Dionysiou and S. C. Pillai, *Nanoscale*, 2016, **8**, 15115–15131.

37 A. Merlo, V. R. S. S. Mokkapati, S. Pandit and I. Mijakovic, *Biomater. Sci.*, 2018, **6**, 2298–2311.

38 C. Lee, J. Drelich and Y. Yap, *Langmuir*, 2009, **25**, 4853–4860.

39 A. Pakdel, C. Zhi, Y. Bando, T. Nakayama and D. Golberg, *ACS Nano*, 2011, **5**, 6507–6515.

40 A. Pakdel, Y. Bando and D. Golberg, *ACS Nano*, 2014, **8**, 10631–10639.

41 D. Liu, M. Zhang, L. He, Y. Chen and W. Lei, *Adv. Mater. Interfaces*, 2017, **4**, 1700392.

42 A. Korycki, F. Chabert, T. Merian and V. Nassiet, *Langmuir*, 2019, **35**, 128–140.